Nano Research
2023, 16(1): 1101–1106
ISSN 1998-0124 CN 11-5974/O4
https://doi.org/10.1007/s12274-022-4685-8

Research Article

Spin-flop transition and Zeeman effect of defect-localized bound states in the antiferromagnetic topological insulator $MnBi_2Te_4$

Guojian Qian[1,§], Mengzhu Shi[3,§], Hui Chen[1,2,§] (✉), Shiyu Zhu[1], Jiawei Hu[1], Zihao Huang[1], Yuan Huang[4], Xian-Hui Chen[3], and Hong-Jun Gao[1,2] (✉)

[1] *Institute of Physics, Chinese Academy of Sciences and University of Chinese Academy of Sciences, Beijing 100190, China*
[2] *Songshan Lake Materials Laboratory, Dongguan 523808, China*
[3] *Hefei National Laboratory for Physical Sciences at Microscale and Department of Physics, and Chinese Academy of Sciences Key Laboratory of Strongly-Coupled Quantum Matter Physics, University of Science and Technology of China, Hefei 230026, China*
[4] *Advanced Research Institute of Multidisciplinary Science, Beijing Institute of Technology, Beijing 100081, China*
[§] *Guojian Qian, Mengzhu Shi, and Hui Chen contributed equally to this work.*

Received: 24 March 2022 / **Revised:** 28 May 2022 / **Accepted:** 21 June 2022

ABSTRACT

The correlation of surface impurity states with the antiferromagnetic ground states is crucial for understanding the formation of the topological surface state in the antiferromagnetic topological insulators $MnBi_2Te_4$. By using low-temperature scanning tunneling microscopy and spectroscopy, we observed a localized bound state around the Mn-Bi antisite defect at the Te-terminated surface of the antiferromagnetic topological insulator $MnBi_2Te_4$. When applying a magnetic field perpendicular to the surface (B_z) from –1.5 to 3.0 T, the bound state shifts linearly to a lower energy with increasing B_z, which is attributed to the Zeeman effect. Remarkably, when applying a large range of B_z from –8.0 to 8.0 T, the magnetic field induced reorientation of surface magnetic moments results in an abrupt jump in the local density of states (LDOS), which is characterized by LDOS-change-ratio $d\tilde{\sigma}/dB$ quantitatively. Interestingly, two asymmetric critical field, –2.0 and 4.0 T determined by the two peaks in $d\tilde{\sigma}/dB$ are observed, which is consistent with simulated results according to a Mills-model, describing a surface spin flop transition (SSF). Our results provide a new flatform for studying the interplay between magnetic order and topological phases in magnetic topological materials.

KEYWORDS

antiferromagnetic topological insulators, $MnBi_2Te_4$, scanning tunneling microscope, Mills model, surface spin flop transition

1 Introduction

The interplay between topology and magnetism generates rich and tunable topological phases [1], which has attracted intensive research interests in condensed matter physics due to the recent discovery of the antiferromagnetic topological insulator $MnBi_2Te_4$ [2–7]. Below T_N = 24 K, the magnetic moments of Mn^{2+}, which point out-of-plane, order ferromagnetically in the *ab*-plane, while they order antiferromagnetically along the *c*-axis [4]. The special magnetic structure (A-type antiferromagnetism) leads to a new class of Z_2 topological insulators which are protected by $S = T_{1/2}\theta$ symmetry, a combination of time-reversal symmetry θ and primitive-lattice translation $T_{1/2}$ [8–10]. Interestingly, at the (0001) surface of $MnBi_2Te_4$, the spontaneously broken S symmetry can also open an exchange gap on the Dirac surface states, which has been observed recently by high-resolution angle-resolved photoemission spectroscopy (ARPES) measurements [3, 5, 11]. In addition to the exchange gap, the interplay between surface magnetization and massless Dirac-like fermions can create the half-quantized Hall effect on the surface [1, 12–17]. Moreover, the topological phase of a $MnBi_2Te_4$ thin film with antiferromagnetic interlayer coupling is predicted to be tuned by the thickness as the sign of the exchange gap is dependent on the orientation of surface magnetization. [10, 18–24]. Recent transport measurements on exfoliated thin flakes provide compelling evidence for these predictions [19–21]. Except for the thickness, the magnetic field can tune the magnetic order, which strongly affects the symmetry, orbital hybridization, and band dispersion of $MnBi_2Te_4$ [13, 22, 23]. Experimentally, the magnetically controllable phase transition from an axion insulator to a Chern insulator with high Chern number or transition from a type II to a type I topological Weyl semimetal [13, 21, 24], have been reported.

Although the quantum anomalous Hall (QAH) state, the axion insulators state, and other topological phases have been confirmed by various measurements, the size of the exchange gap varies in different ARPES measurements, and even gapless surface states were reported [25–29]. A possible explanation for the variation is the surface relaxation especially the reconstruction of surface magnetic order that reduces the gap size. Recently scanning tunneling microscopy (STM) [30–33] and magnetic force microscopy (MFM) [34, 35] revealed the local electronic properties and local magnetic order of the $MnBi_2Te_4$ surface. But

Address correspondence to Hui Chen, hchenn04@iphy.ac.cn; Hong-Jun Gao, hjgao@iphy.ac.cn

the surface states detected by STM are highly inhomogeneous due to the randomly distributed impurities in the sample, and the magnetic response of the electronic states seems irregular [31]. Therefore, it is crucial to understand the electronic properties of local defects at the $MnBi_2Te_4$ surface and their correlation with antiferromagnetic ground states, which to date remained unexplored.

In this Letter, we report the observation of a bound state near the Fermi level which spatially localizes around the Mn-Bi antisite defect at the surface of the $MnBi_2Te_4$ crystal by using low-temperature STM/S. When applying a magnetic field perpendicular to the sample surface (B_z) from –1.5 to 3.0 T, the bound state shifts to lower energy, exhibiting the Zeeman effect of a local moment. When applying a B_z from –8.0 to 8.0 T, the dI/dV spectra show two clear jumps at the transition magnetic field point. Remarkably, the two transition points of surface states are asymmetric, which is attributed to the SSF transition. The SSF transition observed by abrupt transition of electronic states reveals the fact that magnetic order has significant effect on local defect states near the Fermi energy. Our results provide a new platform to explore surface magnetic transition of local moments in the magnetic topological materials with atomic precision.

2 Results and discussion

Intrinsic $MnBi_2Te_4$ is a van der Waals layered material with a rhombohedral crystal structure, formed by ABC-stacked Te-Bi-Te-Mn-Te-Bi-Te septuple layers (SLs) (Fig. 1(a)). Cleaving usually leads to a Te terminated surfaces. In STM images of a Te-terminated surface, the step height is about 1.4 nm (Fig. 1(b)) and the lattice constant of the hexagonal lattice is about 4.3 Å (Fig. 1(d)), consistent with calculated values and previous experimental results [30–33]. Single crystals of $MnBi_2Te_4$ grown by solid-state reaction methods contain a large density of defects [36], which leads to n-doping [37]. Two types of defects are observed in the STM images: the bright spot (labeled by blue dashed circles in Fig. 1(c)) which are Bi-Te antisite defects and the dark triangles (labeled by green dashed triangles in Fig. 1(c)) that correspond to Mn-Bi antisite defects [31, 38–40]. Atomically-resolved STM images show continuously a hexagonal lattice across two types of defects, further confirming the antisite origin underlying the Te surface instead of Te vacancies (Fig. 1(d)). Based on a statistical analysis of the STM images obtained in a 500 nm × 500 nm region, the density of Mn-Bi antisite and Bi-Te antisite defects are estimated to be ~ 3.20% [37] and ~ 0.27%, respectively.

We firstly studied the spatially-averaged electronic properties of the Te-terminated surface by collecting tens of dI/dV spectra over a 100 nm × 100 nm surface region. At the bias voltage from –600 to 100 mV, the spatially-averaged dI/dV spectrum reveals a minimum of the local density of states (LDOS) near –200 mV, indicating n-doping of the samples. At the energy range from –20 to 20 mV, the dI/dV spectrum shows a dip-like feature near the Fermi energy. The significant suppression of DOS near the Fermi level possibly originates from the effect of localization [41].

Next, we focus on the electronic state around the defects near the Fermi level. At the center of a single Mn-Bi antisite defect (Fig. 2(a)), we observed a pronounced conductance peak at 0.3 meV (Fig. 2(b)). The peak intensity gradually decreases when the STM tip is moved away from the center. The decay length of such a conductance peak is about 2 nm. Moreover, the dI/dV map at 0.3 mV further demonstrates that the peak is spatially localized around the Mn-Bi defect (highlighted by the green dashed triangle in Fig. 2(c)), indicating that the conductance peak at 0.3 meV

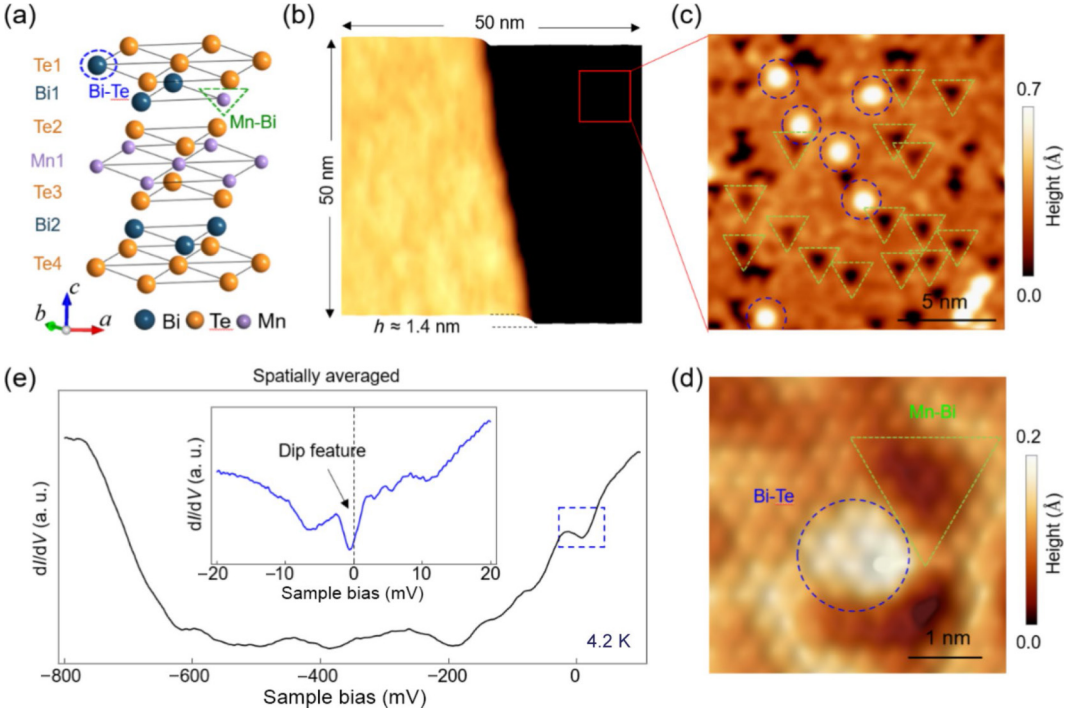

Figure 1 Atomic structure and electronics properties of single crystal of $MnBi_2Te_4$. (a) Schematic diagram of one SL of $MnBi_2Te_4$. Mn_{Bi} antisite defect, where the Mn atom substituting the Bi atom in the second layer (Bi1 layer), is labeled by a green triangle. The Bi_{Te} antisite defect, where the Bi atom substituting the Te atoms in the first layer (Te1 layer), is labelled by a blue circle. (b) A typical STM image (50 nm × 50 nm, setpoint: V_s = –0.5 V, I_t = 10 pA) of Te-terminated surface of $MnBi_2Te_4$. The height of SL terrace step is about 1.4 nm. (c) Zoom-in of (b), showing two types of defects marked by the blue dashed circles and green dashed triangles (4 nm × 4 nm, setpoint: V_s = –10 mV, and I_t = 100 pA). (d) Atomically-resolved STM image of Te-terminated surface (20 nm × 20 nm, V_s = –0.5 V, and I_t = 10 pA), showing a hexagonal lattice structure with lattice constant of a = 4.3 Å. The lattice is continuous across two types of defects, which confirm that the bright defect marked by blue dashed circles is Bi-Te antisites and the dark defect marked by green dashed triangles is Mn-Bi antisites. (e) Spatially averaged dI/dV spectrum obtained at the Te-terminated surface of $MnBi_2Te_4$ (V_s = –800 mV, I_t = 100 pA, and V_{mod} = 5 mV). Inset: low-energy-scale (blue dashed rectangle) and spatially-averaged dI/dV spectrum, showing a clear dip feature near the Fermi level (V_s = 20 mV, I_t = 200 pA, and V_{mod} = 0.1 mV).

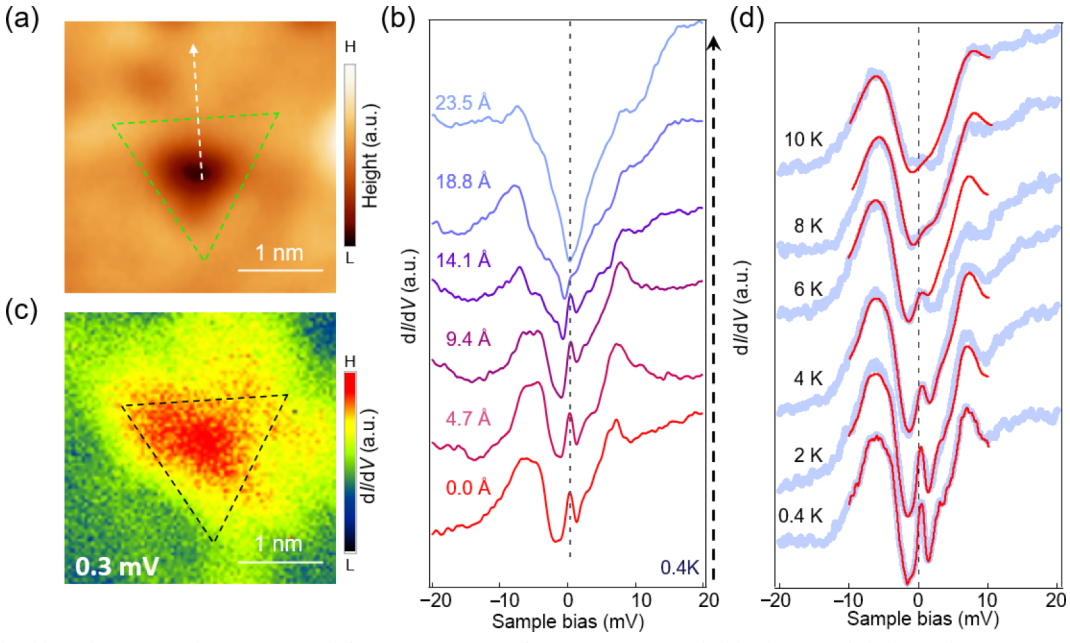

Figure 2 Localized bound state around Mn-Bi antisite defect. (a) STM image of a Mn-Bi antisite marked by the green dashed triangle (V_s = 1.2 V, I_t = 10 pA). (b) Series of dI/dV spectra collected along the white dotted line across Mn-Bi antisite defect in (a), showing that a pronounced bound state near Fermi surface at the defect center is gradually suppressed when moving away from the defect center. The decay length of the bound state is about 2.0 nm (V_s = 10 mV, I_t = 150 pA, and V_{mod} = 0.1 mV). (c) dI/dV map of (a) at the energy of 0.3 meV, showing that bound state is spatially localized around Mn-Bi antisite defect (V_s = 20 mV, I_t = 100 pA, and V_{mod} = 0.1 mV). (d) Temperature-dependent dI/dV spectra collected at the center of Mn-Bi antisite, showing that the bound state is invisible at about 10 K (V_s = 20 mV, I_t = 100 pA, and V_{mod} = 0.1 mV). Red curves are numerically calculated spectra by convoluting the dI/dV spectrum at 0.4 K with the derivative of Fermi–Dirac distribution function at respective temperatures, showing the same evolution behavior with experimental results (light blue curves). Each spectrum in ((b) and (d)) is shifted for clarify.

arises from a localized bound state around the Mn-Bi antisite defect. The observation of a conductance peak is reproduced at most Mn-Bi defects although some of them exhibit complex and vague features which may result from the fluctuation of the local chemical potential, crystal field, and exchange field (Fig. S1 in the Electronic Supplementary Material (ESM)). In contrast, for most Bi-Te antisites, there are no remarkable peak features near the Fermi energy (Fig. S2 in the ESM). Therefore, the peak appearing only at Mn-Bi defects most likely originates from the local magnetic moment of the Mn atom.

The conductance peak near the Fermi energy induced by the magnetic impurity possibly arises from Kondo resonance states [42] or bound states of the impurity potential. To further study the origin of the conductance peak, we obtained temperature dependent dI/dV spectra at the center of Mn-Bi antisite defect. The peak near the Fermi level is substantially suppressed and broadens with increasing temperature, and it disappears at about 10 K (Fig. 2(d)). The red curves in Fig. 2(d) exhibit a series of simulated dI/dV spectra considering solely thermal broadening by convolving the spectrum taken at 0.4 K with the derivative of the Fermi Dirac distribution function of each temperature. The evolution of the peak intensity and peak width in the measured dI/dV spectra with temperature are both in good agreement with the simulated results. Therefore, the intrinsic temperature dependence of the dI/dV spectra, which is only driven by the thermal broadening effect, strongly indicates that the conductance peak results from a localized bound state instead of the Kondo resonance [43] (Fig. 2(d)).

To investigate the magnetic properties of the bound states, we studied the evolution of the dI/dV spectra with the external magnetic field perpendicular to the sample surface (B_z). When increasing B_z from −1.5 to 3.0 T, a clear linear energy shift towards lower energy with increasing magnetic field B_z is observed (Figs. 3(a) and 3(b)). Such a linear shift is well explained by the Zeeman effect of a singly-degenerate spin state. The slope of the Zeeman shift extracted from the fitting line is about −0.15 mV/T which shows that the state has a positive magnetic moment around 2.66 μ_B (Fig. 3(c)). The phenomenon is inconsistent with the picture of a Kondo resonance, where the peak will split with increasing magnetic fields. Therefore, this result demonstrates that the bound state originates from the local moment embedded in the Mn atom of Mn-Bi antisite defect.

Increasing the magnetic field from −8.0 to 8.0 T, the magnetic response of the bound state exhibits a complex behavior beyond the Zeeman effect. In the magnetic field dependent dI/dV spectra, the intensity of occupied states suddenly rises while the intensity of unoccupied states suddenly drops at −2.0 and 4.0 T (Figs. 4(a) and 4(b)). The intensity and energy position of the bound state also suddenly change at the same critical magnetic field. In addition, the transition of LDOS can also be observed at defect-free region (Fig. S3 in the ESM). We attribute the abrupt transition in the B_z-dependent dI/dV spectra to a spin flop transition [44], which means the reorientation of magnetic moments induced by strong magnetic fields. The reorientation of magnetic moments leads to the change of symmetry, interlayer coupling, and local exchange field, which strongly affects the defect states. To quantitatively analyze the evolution of the LDOS and the mechanism behind the transition, we define the rate of change of LDOS with respect to magnetic field

$$\frac{\mathrm{d}\tilde{\sigma}}{\mathrm{d}B} = \frac{\sqrt{\sum\left(\sigma\left(V,B_{i+1}\right)-\sigma\left(V,B_i\right)\right)^2}}{\sum_V\left(\sigma\left(V,B_{i+1}\right)+\sigma\left(V,B_i\right)\right)\times(\Delta B)} \quad (1)$$

where σ is tunneling conductance, B_i is the strength of magnetic field (−8.0 to 8.0 T), V is bias voltage and $\Delta B = |B_{i+1} - B_i|$.

The magnetic field dependence of d$\tilde{\sigma}$/dB (left panel of Fig. 4(c)) shows that there are two peaks in d$\tilde{\sigma}$/dB at −2.0 and +4.0 T which indicates the abrupt transition of the defect state. Moreover, the transition of LDOS at −4.0 and +2.0 T are also observed in another region (Fig. S3 in the ESM). This strange asymmetry of critical field can be well explained by a surface spin flop (SSF)

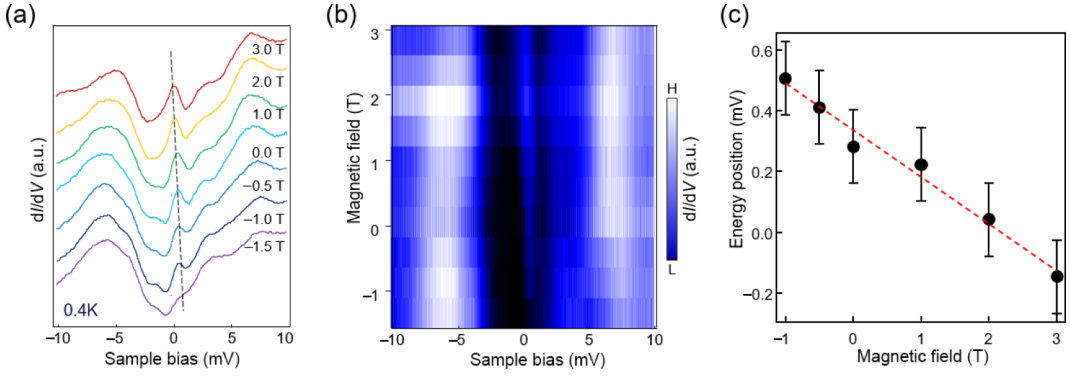

Figure 3 Zeeman effect of the bound state around Mn-Bi antisite defect. (a) Series of d*I*/d*V* spectra obtained at the center of Mn-Bi antisite defect in a magnetic field perpendicular to the sample surface from −1.5 to 3.0 T, showing an approximately linear shift to a lower energy with magnetic field. Moreover, the strength of the impurity state also enhanced with the increasing of magnetic field. Each spectrum is shifted for clarify (V_s = 20 mV, I_t = 100 pA, and V_{mod} = 0.1 mV). (b) Intensity plot of d*I*/d*V* spectra corresponding to (a). (c) Energy shift of the bound state with the magnetic field. The slope of linear fitting (red dotted line) is about −0.15 mV/T which elucidates the state has a positive magnetic moment around 2.66 μ_B. The error bar is the energy resolution of STM.

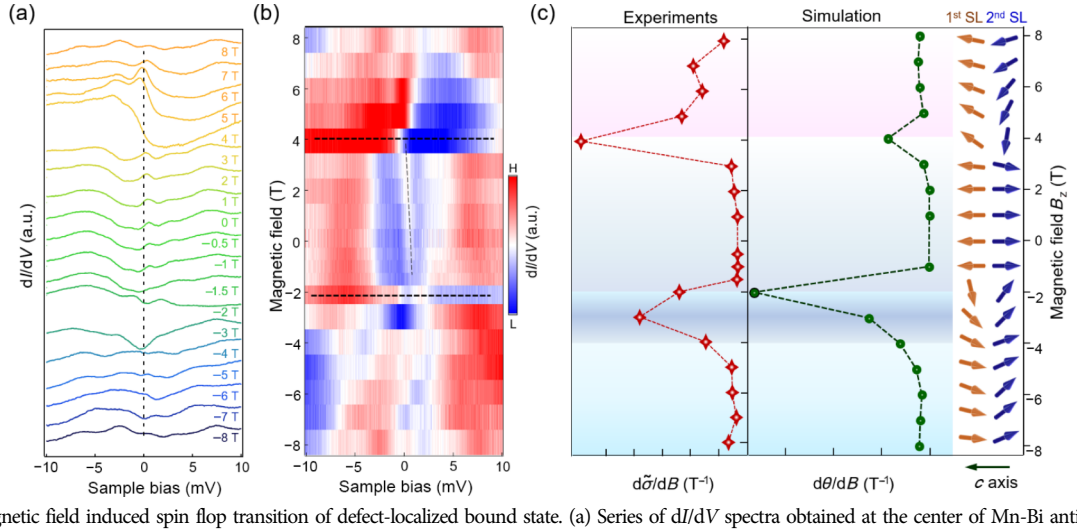

Figure 4 Magnetic field induced spin flop transition of defect-localized bound state. (a) Series of d*I*/d*V* spectra obtained at the center of Mn-Bi antisite defect in a magnetic field perpendicular to the sample surface from −8.0 to 8.0 T, showing two sharp transitions of LDOS at −2.0 and 4.0 T. Each spectrum is shifted for clarify (V_s = 20 mV, I_t = 100 pA, and V_{mod} = 0.1 mV). (b) Intensity plot of d*I*/d*V* spectra corresponding to (a). The two black dashed lines highlight the critical field of LDOS transition. (c) The left panel shows the rate of change of LDOS with magnetic field d$\tilde{\sigma}$/dB, defined by the formula $\sqrt{\sum(\sigma(V,B_{i+1})-\sigma(V,B_i))^2/\sum_V(\sigma(V,B_{i+1})+\sigma(V,B_i))}/(\Delta B)$, which shows the general evolution of d*I*/d*V* spectra with magnetic field. The two sharp peaks indicate two abrupt changes of tunneling spectra which result from the surface spin flop transition. The middle panel is the simulated rate of change of the magnetization dθ/dB of topmost layer according to Mills model, which is consistent with the d$\tilde{\sigma}$/dB measured in experiments. The right panel exhibits the simulated evolution of magnetic moments with magnetic field of the first two layers. The black arrow indicates the *c*-axis of samples.

[44–46]. The opposite critical magnetic fields, (−2.0, 4.0 T) and (−4.0, 2.0 T), observed at different regions are attributed to two distinct (Fig. S4 in the ESM) [36]. For bulk spin flop transition, where the Zeeman energy provided by external magnetic field is large enough to overcome magnetic anisotropic energy and exchange energy, the magnetic moments would be reorientated and lead to a jump of magnetization, whose critical field H_{BSF} is symmetric and about $(2H_EH_K)^{-1/2}$. But for a surface spin flop the exchange stiffness at the topmost surface is weaker than at interior layers, because of cut exchange bonds [45]. Thus, the magnetic moments of the topmost layers are more easily reorientated by external magnetic fields. In addition, magnetic moments of topmost layer antiparallel to the external magnetic field have a relatively weaker critical field (H_{SFA}) compared to parallel orientation (H_{SFP}), shown in the right panel of Fig. 4(c). Considering the bulk spin flop and the surface spin flop simultaneously, there would be three critical field H_{BSF}, H_{SFA}, and H_{SFP}. But because the value of H_{SFP} is very close to H_{BSF}, only two asymmetric critical field −2.0 and 4.0 T can be observed in experiments, which is consistent with the results of MFM experiments (Fig. S4 in the ESM).

The simulated evolution of the magnetic moments of the top two layers according to a Mills model is shown in the right panel of Fig. 4(c), which shows two spin flop transition at −2.0 and +4.0 T. Furthermore, the simulated rate of change of magnetic moments of the topmost layer dθ/dB is consistent with the function d$\tilde{\sigma}$/dB measured in experiments. They both show two sharp peaks at −2.0 and +4.0 T respectively, and the width of the peak at −2.0 T is larger than the width of peak at +4.0 T. These features indicate that the transition of the LDOS is linked with the reorientation of the magnetic order, which in turn confirms our conjecture about a spin flop induced LDOS transition. Amalgamated with the Zeeman shift of impurity states with magnetic field, we claim that the magnetic response of impurity states is the sum of Zeeman effect and surface spin flop transition.

3 Conclusions

We studied the intrinsic defect states in the antiferromagnetic topological insulator $MnBi_2Te_4$ using STM/S at 400 mK. We observed a bound state near the Fermi energy localized around Mn-Bi antisites. The defect-localized bound state shows a clear linear energy shift with magnetic field B_z from −1.5 to 3.0 T. And the slope of Zeeman shift indicates that the state has a positive

magnetic moment of around 2.66 μ_B. Increasing B_z from −8.0 to 8.0 T, the LDOS changes drastically at two critical field strengths. The phase diagram of the LDOS transition reveals two asymmetric critical fields at −2.0 and +4.0 T, respectively, which can be attributed to the phenomenon of a surface spin flop. Due to the exchange cut, the critical field is weaker when the magnetic moments of the topmost layer are antiparallel to external magnetic field. Our results reveal that the magnetic responses of $MnBi_2Te_4$ are the sum of a Zeeman effect and a spin flop transition and provide a new paradigm for studying the interplay between surface magnetic transition and local defect states.

4 Methods

4.1 Crystal growth

The $MnBi_2Te_4$ crystals were synthesized through a solid state reaction of Mn powder, Bi lump, and Te lump followed by a water quenching process. Mn powder, Bi lump, and Te lump were mixed with the molar ratio of 1:2:4 into the silica container in an argon gas glovebox. The above mixture was sealed and reacted in a self-built vertical Bridgman furnace. The temperature was ramped to 1,100 °C in 400 min, which was kept for 48 h; then the temperature was cooled to 900 °C in 48 h and further cooled to 700 °C in 72 h, which was kept for another 72 h. Finally, the ampoule was quenched in water quickly. $MnBi_2Te_4$ single crystals could be cleaved from the product.

4.2 STM/STS

The $MnBi_2Te_4$ samples were cleaved *in situ* at room temperature and immediately transferred into a STM head. The STM/S experiments were performed in an ultrahigh vacuum (1×10^{-11} mbar) LT-STM system (USM-1300-^{3}He), which can apply a magnetic field perpendicular to the sample surface up to 11.0 T. STM images were acquired in the constant-current mode with a tungsten tip. The STM tips were calibrated on a Au(111) surface before measurements. Differential conductance (dI/dV) spectra were acquired by a standard lock-in amplifier at a frequency of 973.0 Hz under the modulation voltage as labeled.

4.3 MFM

The MFM experiments were carried out in a commercial cryogenic magnetic force microscope using cobalt alloy coating MFM tips at 4.2 K. MFM images were taken in a constant height mode with the scanning plane nominally ~ 200 nm above the sample surface.

4.4 Monte Carlo simulation

The Monte Carlo simulations of an antiferromagnetic superlattice were based on Mills model. In Mills model, we consider a stack of N ferromagnetic plates with magnetizations m_i and antiferromagnetic interlayer couplings. To calculate the one-dimensional configurations, one can replace this by a linear chain of coupled unity vector spins $s_i = m_i/|m_i|$

$$\widehat{H} = \sum_{i=0}^{N-1} J \cdot \mathrm{s}_i \cdot \mathrm{s}_j + \sum_{i=1}^{N} B \cdot \mathrm{s}_i - \sum_{i=1}^{N} \frac{K}{2} \cdot (\mathrm{s}_i^z)^2 \quad (2)$$

where the magnetic moments at layer i and j are described by unit vectors s_i and s_j respectively. The magnetic coupling constant J = 0.14, and the magnetic anisotropy K = 0.05. The number of layers (N) was set to be 20 for phase diagram simulations.

Acknowledgements

We thank Werner A. Hofer for critical reading of the manuscript and Ziqiang Wang for helpful discussion. This work is supported by the National Natural Science Foundation of China (Nos. 61888102 and 52022105), National Key Research and Development Projects of China (Nos. 2018YFA0305800 and 2019YFA0308500), the Strategic Priority Research Program of Chinese Academy of Sciences (Nos. XDB30000000 and XDB28000000), CAS Project for Young Scientists in Basic Research (No. YSBR-003), and the University of Chinese Academy of Sciences.

Electronic Supplementary Material: Supplementary material (additional STM measurement on Mn-Bi antisite defects and MFM measurement on surface magnetic transition) is available in the online version of this article at https://doi.org/10.1007/s12274-022-4685-8.

References

[1] Tokura, Y.; Yasuda, K.; Tsukazaki, A. Magnetic topological insulators. *Nat. Rev. Phys.* **2019**, *1*, 126–143.

[2] Li, J. H.; Li, Y.; Du, S. Q.; Wang, Z.; Gu, B. L.; Zhang, S. C.; He, K.; Duan, W. H.; Xu, Y. Intrinsic magnetic topological insulators in van der Waals layered $MnBi_2Te_4$-family materials. *Sci. Adv.* **2019**, *5*, eaaw5685.

[3] Otrokov, M. M.; Klimovskikh, I. I.; Bentmann, H.; Estyunin, D.; Zeugner, A.; Aliev, Z. S.; Gaß, S.; Wolter, A. U. B.; Koroleva, A. V.; Shikin, A. M. et al. Prediction and observation of an antiferromagnetic topological insulator. *Nature* **2019**, *576*, 416–422.

[4] Yan, J. Q.; Zhang, Q.; Heitmann, T.; Huang, Z. L.; Chen, K. Y.; Cheng, J. G.; Wu, W. D.; Vaknin, D.; Sales, B. C.; McQueeney, R. J. Crystal growth and magnetic structure of $MnBi_2Te_4$. *Phys. Rev. Mater.* **2019**, *3*, 064202.

[5] Rienks, E. D. L.; Wimmer, S.; Sánchez-Barriga, J.; Caha, O.; Mandal, P. S.; Růžička, J.; Ney, A.; Steiner, H.; Volobuev, V. V.; Groiss, H. et al. Large magnetic gap at the Dirac point in Bi_2Te_3/$MnBi_2Te_4$ heterostructures. *Nature* **2019**, *576*, 423–428.

[6] Lee, D. S.; Kim, T. H.; Park, C. H.; Chung, C. Y.; Lim, Y. S.; Seo, W. S.; Park, H. H. Crystal structure, properties and nanostructuring of a new layered chalcogenide semiconductor, Bi_2MnTe_4. *CrystEngComm* **2013**, *15*, 5532–5538.

[7] Zhang, D. Q.; Shi, M. J.; Zhu, T. S.; Xing, D. Y.; Zhang, H. J.; Wang, J. Topological axion states in the magnetic insulator $MnBi_2Te_4$ with the quantized magnetoelectric effect. *Phys. Rev. Lett.* **2019**, *122*, 206401.

[8] Mong, R. S. K.; Essin, A. M.; Moore, J. E. Antiferromagnetic topological insulators. *Phys. Rev. B* **2010**, *81*, 245209.

[9] Fang, C.; Gilbert, M. J.; Bernevig, B. A. Topological insulators with commensurate antiferromagnetism. *Phys. Rev. B* **2013**, *88*, 085406.

[10] Otrokov, M. M.; Rusinov, I. P.; Blanco-Rey, M.; Hoffmann, M.; Vyazovskaya, A. Y.; Eremeev, S. V.; Ernst, A.; Echenique, P. M.; Arnau, A.; Chulkov, E. V. Unique thickness-dependent properties of the van der Waals interlayer antiferromagnet $MnBi_2Te_4$ films. *Phys. Rev. Lett.* **2019**, *122*, 107202.

[11] Shikin, A. M.; Estyunin, D. A.; Zaitsev, N. L.; Glazkova, D.; Klimovskikh, I. I.; Filnov, S. O.; Rybkin, A. G.; Schwier, E. F.; Kumar, S.; Kimura, A. et al. Sample-dependent Dirac-point gap in $MnBi_2Te_4$ and its response to applied surface charge: A combined photoemission and *ab initio* study. *Phys. Rev. B* **2021**, *104*, 115168.

[12] Qi, X. L.; Zhang, S. C. Topological insulators and superconductors. *Rev. Mod. Phys.* **2011**, *83*, 1057–1110.

[13] He, K. $MnBi_2Te_4$-family intrinsic magnetic topological materials. *npj Quantum Mater.* **2020**, *5*, 90.

[14] Qi, X. L.; Hughes, T. L.; Zhang, S. C. Topological field theory of time-reversal invariant insulators. *Phys. Rev. B* **2008**, *78*, 195424.

[15] Wilczek, F. Two applications of axion electrodynamics. *Phys. Rev. Lett.* **1987**, *58*, 1799–1802.

[16] Essin, A. M.; Moore, J. E.; Vanderbilt, D. Magnetoelectric polarizability and axion electrodynamics in crystalline insulators. *Phys. Rev. Lett.* **2009**, *102*, 146805.

[17] Liu, C. X.; Zhang, S. C.; Qi, X. L. The quantum anomalous hall effect: Theory and experiment. *Annu. Rev. Condens. Matter Phys.* **2016**, *7*, 301–321.

[18] Yu, R.; Zhang, W.; Zhang, H. J.; Zhang, S. C.; Dai, X.; Fang, Z. Quantized anomalous hall effect in magnetic topological insulators. *Science* **2010**, *329*, 61–64.

[19] Deng, Y. J.; Yu, Y. J.; Shi, M. Z.; Guo, Z. X.; Xu, Z. H.; Wang, J.; Chen, X. H.; Zhang, Y. B. Quantum anomalous hall effect in intrinsic magnetic topological insulator $MnBi_2Te_4$. *Science* **2020**, *367*, 895–900.

[20] Liu, C.; Wang, Y. C.; Li, H.; Wu, Y.; Li, Y. X.; Li, J. H.; He, K.; Xu, Y.; Zhang, J. S.; Wang, Y. Y. Robust Axion insulator and Chern insulator phases in a two-dimensional antiferromagnetic topological insulator. *Nat. Mater.* **2020**, *19*, 522–527.

[21] Ge, J.; Liu, Y. Z.; Li, J. H.; Li, H.; Luo, T. C.; Wu, Y.; Xu, Y.; Wang, J. High-Chern-number and high-temperature quantum hall effect without landau levels. *Natl. Sci. Rev.* **2020**, *7*, 1280–1287.

[22] Li, J. H.; Wang, C.; Zhang, Z. T.; Gu, B. L.; Duan, W. H.; Xu, Y. Magnetically controllable topological quantum phase transitions in the antiferromagnetic topological insulator $MnBi_2Te_4$. *Phys. Rev. B* **2019**, *100*, 121103.

[23] Klimovskikh, I. I.; Otrokov, M. M.; Estyunin, D.; Eremeev, S. V.; Filnov, S. O.; Koroleva, A.; Shevchenko, E.; Voroshnin, V.; Rybkin, A. G.; Rusinov, I. P. et al. Tunable 3D/2D magnetism in the $(MnBi_2Te_4)$ $(Bi_2Te_3)_m$ topological insulators family. *npj Quantum Mater.* **2020**, *5*, 54.

[24] Lee, S. H.; Graf, D.; Min, L. J.; Zhu, Y. L.; Yi, H. M.; Ciocys, S.; Wang, Y. X.; Choi, E. S.; Basnet, R.; Fereidouni, A. et al. Evidence for a magnetic-field-induced ideal type-II Weyl state in antiferromagnetic topological insulator $Mn(Bi_{1-x}$ $Sb_x)_2Te_4$. *Phys. Rev. X* **2021**, *11*, 031032.

[25] Li, H.; Gao, S. Y.; Duan, S. F.; Xu, Y. F.; Zhu, K. J.; Tian, S. J.; Gao, J. C.; Fan, W. H.; Rao, Z. C.; Huang, J. R. et al. Dirac surface states in intrinsic magnetic topological insulators $EuSn_2As_2$ and $MnBi_{2n}Te_{3n+1}$. *Phys. Rev. X* **2019**, *9*, 041039.

[26] Swatek, P.; Wu, Y.; Wang, L. L.; Lee, K.; Schrunk, B.; Yan, J. Q.; Kaminski, A. Gapless Dirac surface states in the antiferromagnetic topological insulator $MnBi_2Te_4$. *Phys. Rev. B* **2020**, *101*, 161109.

[27] Yan, C. H.; Sebastian F.-M.; Mei, R. B.; Lee, S. H.; Nikola P.; Rikuto F.; Yan, B. H.; Liu, C. X.; Mao, Z. Q.; Yang, S. L. Origins of electronic bands in the antiferromagnetic topological insulator $MnBi_2Te_4$. *Phys. Rev. B* **2021**, *104*, L041102.

[28] Hao, Y. J.; Liu, P. F.; Feng, Y.; Ma, X. M.; Schwier, E. F.; Arita, M.; Kumar, S.; Hu, C. W.; Lu, R.; Zeng, M. et al. Gapless surface Dirac cone in antiferromagnetic topological insulator $MnBi_2Te_4$. *Phys. Rev. X* **2019**, *9*, 041038.

[29] Chen, Y. J.; Xu, L. X.; Li, J. H.; Li, Y. W.; Wang, H. Y.; Zhang, C. F.; Li, H.; Wu, Y.; Liang, A. J.; Chen, C. et al. Topological electronic structure and its temperature evolution in antiferromagnetic topological insulator $MnBi_2Te_4$. *Phys. Rev. X* **2019**, *9*, 041040.

[30] Wu, X. F.; Li, J. Y.; Ma, X. M.; Zhang, Y.; Liu, Y. T.; Zhou, C. S.; Shao, J. F.; Wang, Q. M.; Hao, Y. J.; Feng, Y. et al. Distinct topological surface states on the two terminations of $MnBi_4Te_7$. *Phys. Rev. X* **2020**, *10*, 031013.

[31] Yuan, Y. H.; Wang, X. T.; Li, H.; Li, J. H.; Ji, Y.; Hao, Z. Q.; Wu, Y.; He, K.; Wang, Y. Y.; Xu, Y. et al. Electronic states and magnetic response of $MnBi_2Te_4$ by scanning tunneling microscopy and spectroscopy. *Nano Lett.* **2020**, *20*, 3271–3277.

[32] Liang, Z. W. ; Luo, A. Y. ; Shi, M. Z. ; Zhang, Q. ; Nie, S. M. ; Ying, J. J. ; He, J. F. ; Wu, T. ; Wang, Z. J. ; Xu, G. et al. Mapping Dirac fermions in the intrinsic antiferromagnetic topological insulators $(MnBi_2Te_4)$ $(Bi_2Te_3)_n$ (n = 0, 1). *Phys. Rev. B* **2020**, *102*, 161115(R).

[33] Ko, W.; Kolmer, M.; Yan, J. Q.; Pham, A. D.; Fu, M. M.; Lüpke, F.; Okamoto, S.; Gai, Z.; Ganesh, P.; Li, A. P. Realizing gapped surface states in the magnetic topological insulator $MnBi_{2-x}Sb_xTe_4$. *Phys. Rev. B* **2020**, *102*, 115402.

[34] Sass, P. M.; Ge, W. B.; Yan, J. Q.; Obeysekera, D.; Yang, J. J.; Wu, W. D. Magnetic imaging of domain walls in the antiferromagnetic topological insulator $MnBi_2Te_4$. *Nano Lett.* **2020**, *20*, 2609–2614.

[35] Sass, P. M.; Kim, J.; Vanderbilt, D.; Yan, J. Q.; Wu, W. D. Robust A-type order and spin-flop transition on the surface of the antiferromagnetic topological insulator $MnBi_2Te_4$. *Phys. Rev. Lett.* **2020**, *125*, 037201.

[36] Cui, J. H.; Shi, M. Z.; Wang, H. H.; Yu, F. H.; Wu, T.; Luo, X. G.; Ying, J. J.; Chen, X. H. Transport properties of thin flakes of the antiferromagnetic topological insulator $MnBi_2Te_4$. *Phys. Rev. B* **2019**, *99*, 155125.

[37] Zeugner, A.; Nietschke, F.; Wolter, A. U. B.; Gaß, S.; Vidal, R. C.; Peixoto, T. R. F.; Pohl, D.; Damm, C.; Lubk, A.; Hentrich, R. et al. Chemical aspects of the candidate antiferromagnetic topological insulator $MnBi_2Te_4$. *Chem. Mater.* **2019**, *31*, 2795–2806.

[38] Netsou, A. M.; Muzychenko, D. A.; Dausy, H.; Chen, T. S.; Song, F. Q.; Schouteden, K.; Van Bael, M. J.; Van Haesendonck, C. Identifying native point defects in the topological insulator Bi_2Te_3. *ACS Nano* **2020**, *14*, 13172–13179.

[39] Huang, Z. L. ; Du, M. H. ; Yan, J. Q. ; Wu, W. D. Native defects in antiferromagnetic topological insulator $MnBi_2Te_4$. *Phys. Rev. Mater.* **2020**, *4*, 121202(R).

[40] Lee, I. ; Kim, C. K. ; Lee, J. ; Billinge, S. J. L. ; Zhong, R. D. ; Schneeloch, J. A. ; Liu, T. S. ; Valla, T. ; Tranquada, J. M. ; Gu, G. D. et al. Imaging Dirac-mass disorder from magnetic dopant atoms in the ferromagnetic topological insulator $Cr_x(Bi_{0.1}Sb_{0.9})_{2-x}Te_3$. *Proc. Natl. Acad. Sci. USA* **2015**, *112*, 1316–1321.

[41] Jeon, S.; Kim, S.; Kuk, Y. Zero-bias anomaly and role of electronic correlations in a disordered metal film. *New J. Phys.* **2020**, *22*, 083045.

[42] Madhavan, V.; Chen, W.; Jamneala, T.; Crommie, M. F.; Wingreen, N. S. Local spectroscopy of a Kondo impurity: Co on Au(111). *Phys. Rev. B* **2001**, *64*, 165412.

[43] Nagaoka, K.; Jamneala, T.; Grobis, M.; Crommie, M. F. Temperature dependence of a single Kondo impurity. *Phys. Rev. Lett.* **2002**, *88*, 077205.

[44] Mills, D. L. Surface spin-flop state in a simple antiferromagnet. *Phys. Rev. Lett.* **1968**, *20*, 18–21.

[45] Rößler, U. K.; Bogdanov, A. N. Reorientation in antiferromagnetic multilayers: Spin‐flop transition and surface effects. *Phys. Stat. Sol. (c)* **2004**, *1*, 3297–3305.

[46] Bogdanov, A. N.; Rößler, U. K. Magnetic-field-induced reorientation in thin antiferromagnetic films: Spin-flop transition and surface-induced twist effects. *Phys. Rev. B* **2003**, *68*, 012407.